



Theoretical and experimental studies of spindle ball bearing nonlinear stiffness

Mohammad Faraji Ghanati and Reza Madoliat[‡]

Iran University of Science and Technology (IUST), Narmak, Tehran, Iran 16846

The following study concentrates on nonlinear stiffness of milling machine tool spindle angle contact ball bearings in static mode. As a primarily theoretical study, it allowed us to build an analytical model to define nonlinear stiffness of angle contact ball bearings based on geometrical and physical parameters. Ball bearing deformation is also considered. Modifications were made to literature models resulting in better conformity of models to experimental results. An FEM model using ANSYS was constructed to analyze the different parameters' effects on nonlinear stiffness of ball bearings. Among those parameters are physical ones, including the geometry, friction coefficient and boundary conditions, and numerical parameters such as mesh density and penetration. Experimental tests were done on the spindle ball bearing 7014 to measure the rigidity. A universal tensile testing machine was used to achieve the load-displacement curve. Experimental results were compared to the theoretical model. The developed theoretical model, constructed finite-element model, and experimental results showed good conformity.

KEYWORDS: Modeling; ball bearing; stiffness; FEM modeling

COPYRIGHT: © 2013 Ghanati. This is an open-access article distributed under the terms of the Creative Commons Attribution License, which permits unrestricted use, distribution, and preproduction in any medium, provided the original author and source are credited.

The behavior of ball bearings is based on the stiffness calculation from local Hertz deformation [1]. Early research by Palmgren [2], Harris [3] and Eschmann *et al.* [4] focused on structural nonlinearities associated with the ball bearings because of mechanical gaps, Hertzian local contacts between balls and races and lubrication, among other topics. Palmgren established an analytical model of ball bearings from a “force-displacement” viewpoint. Recently, other models have been developed based on FEM methods. Lim [5] proposed a matrix model and validated the results by experiments on other literature models. De Mul *et al.* [6] used the same model of Lim but analysis was

based on vectorial description. Fukata *et al.* [7] proposed a model which considers the ball's inertia. Our contribution to this research is to suggest a different approach from existing works to obtain a ball bearing static stiffness model. The majority of preceding works ([2]-[9], [15]-[17]) are based on the Hertz theory but in the current study, we introduce a different approach by calculating deformations analytically. This study is also different in that the dynamic stiffness calculation is usually obtained by analytical calculation without experimental check [10]. However, Bogard *et al.* [11] and Marsh [14] have shown that the analytical model presents difficulties and gives bad answers to the dynamic calculation requirements. Therefore experimental methods to measure dynamic stiffness are necessary to support theoretical findings.

Yuan *et al.* [18] present stiffness function for all angular-contact ball bearings by a back-propagation neural network method, which is trained by using

[‡]Correspondence: madoliat@iust.ac.ir

Received: 19 April 2012; Accepted: 13 September 2012

several (but not all) samples. Sayed [19] derived an equation for predicting the stiffness of deep-groove ball bearings. Experimental verification showed that the predicted results are satisfactory. In Guo's work [20], a combined surface integral and finite element method is used to solve for the contact mechanics between the rolling elements and races. This model captures the time-dependent characteristics of the bearing contact due to the orbital motion of the rolling elements. Aydin [21] investigates the role of bearing preloads on the modal characteristics of a shaft-bearing assembly with a double row angular contact ball bearing. In Chen's research [22] the stiffness of various geometric designs of aerostatic journal bearings for high-speed spindles was investigated under different operating conditions. Stone's work [23] presented the methods and results of three research groups which have investigated the stiffness and damping of rolling element bearings whereby the most significant parameters are shown to be type of bearing, axial preload, clearance/interference, speed and lubricant. Harsha [24] presents an analytical model to investigate the nonlinear dynamic behavior due to cage run-out and number of balls in a rotating system supported by rolling element bearings.

To study different physical and analytical parameters such as ball diameter, friction coefficient, penetration effects and boundary conditions in rigidity of ball bearing's FEM model was developed using ANSYS workbench. Moreover, we have experimentally checked the static stiffness model and compared our model results to some existing models found in the literature.

1. Stiffness modeling

The theoretical development of ball bearing model requires a contact mechanism, an equivalent model loading, and boundary conditions.

Calculation procedure

Deformations are calculated as a function of applied loads in order to deduce the stiffness. The ball bearing total deformation is composed of the local deformation due to contact of the ball to the outer and inner rings and balls and the ring's global elastic deformation. In this study, we concentrate only on the radial stiffness calculation of ball bearing. To obtain stiffness, the local deformation resulting from the contact between the ball and ring and global deformation of balls is considered. While

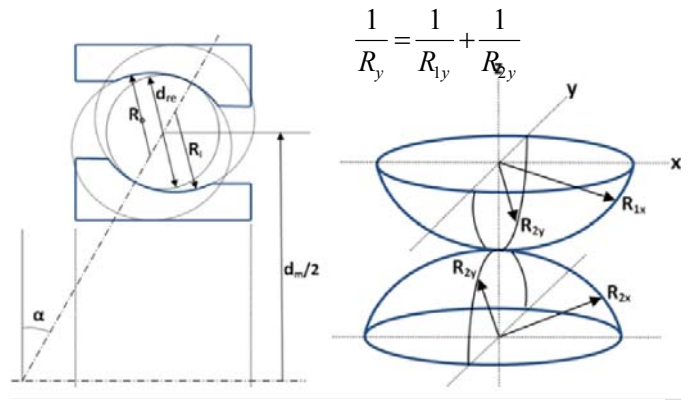


Figure 1. Contact bodies in an angle contact ball bearing

other parameters affect the global deformation (*e.g.* elasticity of rings and housings), our experimental setup designed in such a way that only these two types of deformations were analyzed.

1.1 Calculation according to the Hertz model

If R_{re} denotes the radius of the ball, the radii of the curvature for the inner contact is (fig. 1) [1]:

$$\begin{aligned} R_{1x} &= R_{re} \\ R_{1y} &= R_{re} \\ R_{2x} &= \frac{d_m/2}{\cos(\alpha)} - R_{re} \\ R_{2y} &= -R_i \end{aligned} \quad (1)$$

Where:

- R_{1x}, R_{1y} : Radii of the ball in two different planes
- R_{2x}, R_{2y} : Radii of the inner race in two different planes
- α : Ball bearing contact angle
- d_m : Ball rotation diameter

Two contacting solids formulations is expressed in terms of the curvature sum R , and curvature difference R_d :

$$\frac{1}{R} = \frac{1}{R_x} + \frac{1}{R_y} \quad (2)$$

$$\frac{1}{R_d} = R \left(\frac{1}{R_x} - \frac{1}{R_y} \right) \quad (3)$$

Where

$$\frac{1}{R_x} = \frac{1}{R_{1x}} + \frac{1}{R_{2x}} \quad (4)$$

$$\frac{1}{R_y} = \frac{1}{R_{1y}} + \frac{1}{R_{2y}} \quad (5)$$

An ellipse is created in ball and race contact point in load application where a and b are semi-minor and semi-major axes of this ellipse geometry. The ellipticity parameter k_e is defined as (Reusner,1977):

$$k_e = \frac{a}{b} \tag{6}$$

Also this parameter can be defined as a function of curvature difference R_d and the elliptic integrals of the first ξ and second ζ kind as:

$$k_e = \left[\frac{2\xi - \zeta(1+R_d)}{\zeta(1-R_d)} \right]^{1/2} \tag{7}$$

Where

$$\xi = \int_0^{\pi/2} \left[1 - \left(1 - \frac{1}{k_e^2}\right) \sin^2 \varphi \right]^{-1/2} d\varphi \tag{8}$$

$$\zeta = \int_0^{\pi/2} \left[1 - \left(1 - \frac{1}{k_e^2}\right) \sin^2 \varphi \right]^{1/2} d\varphi \tag{9}$$

Where φ is an auxiliary angle. As can be seen, integration is required to determine the ellipticity parameter and elliptic integrals. Numerical iteration and curve fitting techniques are followed to determine the ellipticity parameter:

$$\bar{k}_e = 1.0339 \left(\frac{R_y}{R_x} \right)^{0.6360} \tag{10}$$

$$\bar{\xi} = 1.0003 + 0.5968 \frac{R_x}{R_y} \tag{11}$$

$$\bar{\zeta} = 1.5277 + 0.6023 \ln \left(\frac{R_y}{R_x} \right) \tag{12}$$

The contact stiffness coefficient for the elliptical contact assumption can be calculated as:

$$K_c = \pi \bar{k}_e A E' \sqrt{\frac{R \bar{\xi}}{4.5 \bar{\zeta}^3}} \tag{13}$$

Where the effective modulus of elasticity, E' , is defined as:

$$\frac{1}{E'} = \frac{1}{2} \left(\frac{1-\nu_1^2}{E_1} + \frac{1-\nu_2^2}{E_2} \right) \tag{14}$$

E is the modulus of elasticity and ν is Poisson's ratio. Subscripts denote solids 1 and 2. In the case of the ball bearing, both of the solids have the same elasticity properties.

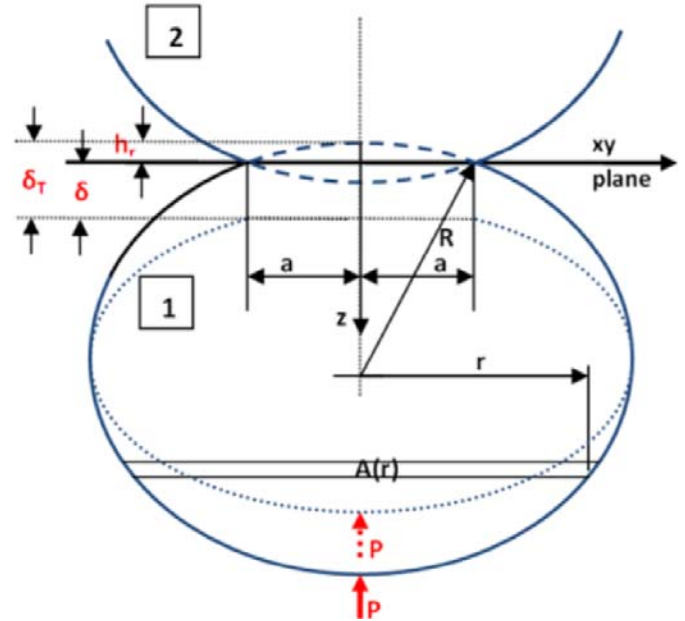


Figure 2. Local and total deformation of a ball

1.2 Calculation based on total deformation

In the new method introduced here, the ball's elastic deformation as well as local Hertzian deformation is considered for calculation. Hertzian deformation of one side is given by h_r (fig. 2) for a contact between ball and ring as calculated geometrically:

$$h_r = R - \sqrt{R^2 - a^2} \tag{15}$$

According to equations 6-9, a can be calculated as below:

$$a = \left(\frac{6k_e^2 \zeta R F}{\pi E'} \right)^{1/3} \tag{16}$$

This is a new formula according to geometric interpretation, ellipticity parameter, and elliptic integrals of the first and second integrals. To compare this result with the, literature below comments should be kept in mind.

Hertz's law gives the deformation in the following form:

$$\delta = \frac{\pi a p_0}{2E^*} \tag{17}$$

$$a = \sqrt[3]{\frac{3F [(1-\nu_1^2)/E_1] + [(1-\nu_2^2)/E_2]}{8 (1/d_1) + (1/d_2)}} \tag{17}$$

With:

$$\frac{1}{E^*} = \frac{1-\nu_1^2}{E_1} + \frac{1-\nu_2^2}{E_2} \text{ and } p_0 = \frac{3F}{2\pi a^2} \text{ (Shigley, 1983)} \tag{18}$$

If δ is formulated as in **equation 17** by using a as in Palmgren [2], Lim and Chin [5], De Mul *et al.* [6] we obtain the force-displacement relation:

$$F = K\delta_h^{3/2} \tag{19}$$

Where K is the stiffness factor. **Equations 15, 16 and 19** have the similar bases, but in the new method deformation h_r is obtained geometrically. Using the new method, the total deformation and force-displacement relation can be calculated easily. Using Timoshenko (1968) beam theory and Hooke's law, we modeled the ball compression. The elastic deformation of the ball is calculated as:

$$\frac{d\delta}{dr} = \frac{F}{EA(r)} \tag{20}$$

By resolving the equation in symmetrical domain of r (o..((R - h_r)) as shown in **figure 2** and adding local deformation between ball-inner race and ball-outer race contact, the total deformation formula including both elastic deformation of the ball and local Hertzian deformations is obtained as follows:

$$\delta_r = \left(\frac{F}{\pi E d_b} \ln \left[\frac{d_b}{h_r} - 1 \right] \right) + h_r + h'_r \tag{21}$$

Where h'_r is the local deformation between outer race and ball that is calculated the same as contact between ball and inner race but with different curvatures.

Equation 21 permits adopting a method to construct the curve of force-displacement $f(\delta_r)$. We have for each applied force F_i a corresponding local deformation h_r and h'_r using **equation 15**. Then these local deformations are introduced in **equation 21** to obtain the corresponding total deformation δ_r .

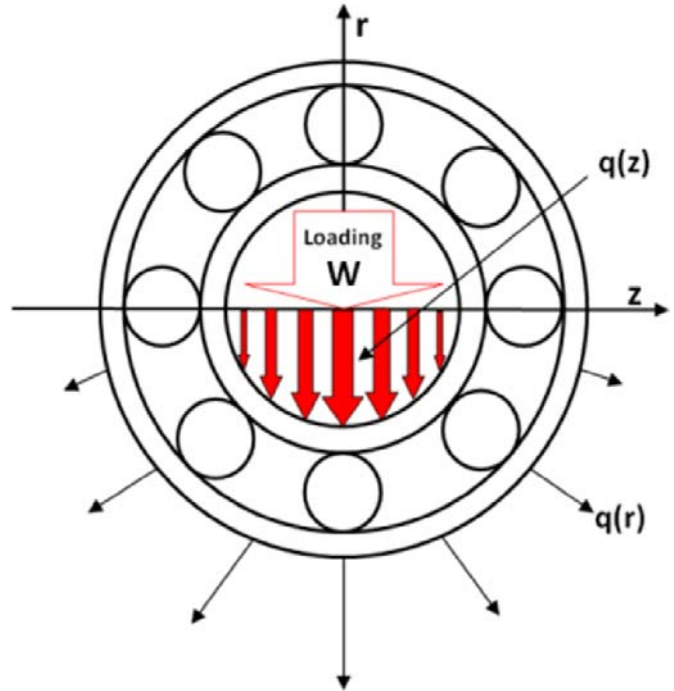


Figure 3. Force distribution on loaded balls

The distributed loading on a ball bearing is illustrated in **figures 4 and 5** for a distributed loading slice on one ball between $(\varphi_i \varphi_{i+1})$, we have the following form (**fig. 3**):

$$q(\varphi) = q_0 \sqrt{1 - \cos^2(\varphi)} = q_0 \cdot \sin \varphi \tag{22}$$

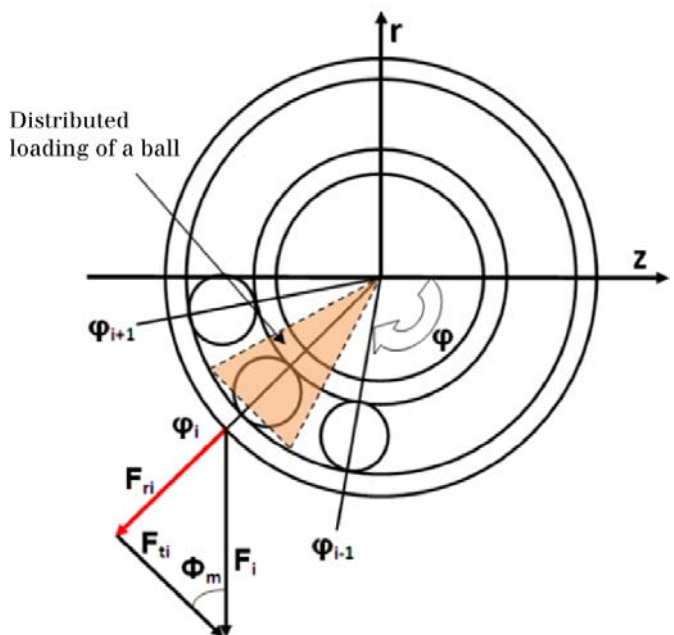


Figure 4. The loading component of a ball

The total loading F_i applied to i^{2nd} ball is:

$$F_i = Lc \int_{Z_i}^{Z_{i+1}} q(Z) dZ = LcRq_0 \int_{\varphi_i - \frac{\varphi_n}{2}}^{\varphi_i + \frac{\varphi_n}{2}} -\sin \varphi^2 d\varphi \quad (23)$$

After resolution of **equation 23** for:

$$\varphi_n = \frac{2\pi}{n}$$

and

$$q_0 = \frac{2F}{RL_c\pi}$$

$$F_i = \frac{F}{2\pi} \left[\sin 2 \left(\varphi_i + \frac{\pi}{n} \right) - \sin 2 \left(\varphi_i - \frac{\pi}{n} \right) - \frac{4\pi}{n} \right] \quad (24)$$

The radial load is defined by:

$$F_r = |F_i| \sin \varphi_m \quad (25)$$

$$\varphi_m = \frac{\varphi_i + \varphi_{i+1}}{2}$$

The law linking loads to deformation [15] is expressed as follows:

$$K_{rr}^{(b)} = \frac{dF_r}{d\delta_r} \quad (26)$$

Using **equation 21** the force-displacement curve f_r is obtained. Using **equation 26**, the ball stiffness for the nominal loading on each ball expressed by:

$$K_r = \frac{F_r}{2 \cdot \frac{F}{\pi E d_b} \ln \left[\frac{d_b}{h_r} - 1 \right] + 4 \cdot h_r} \quad (27)$$

To obtain the total ball bearing radial stiffness, all loaded balls are considered. These are not uniformly loaded and their positioning in the cage is changing due to the ball bearing kinematics, and consequently stiffness is varying. The stiffness therefore becomes dependent on position.

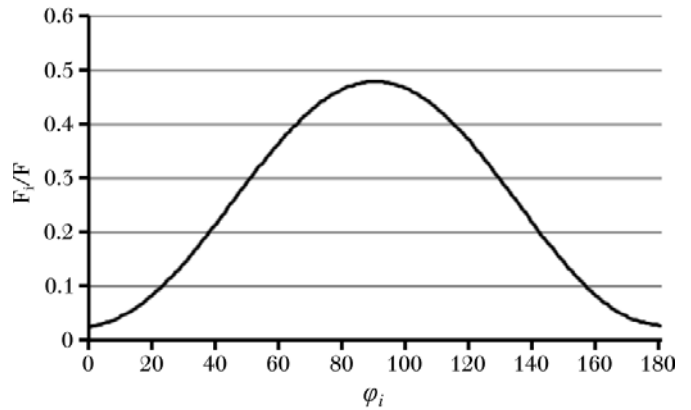


Figure 5. Applied force for a ball at position φ_i

2. The Palmgren and Kramer models

The most important research in the field of stiffness calculation of ball bearing was conducted by Palmgren [2] and Kramer [9]. The results of their works are hence compared with the model developed in this paper and experimental results are presented in the following section.

2.1 The Palmgren formula

Loads in rolling elements are given as follows [2]:

$$Q = \frac{5F_r}{i \cdot Z \cdot \cos \beta} \quad (28)$$

Balls: $\delta_r = 0.0020Q^{2/3}D_w^{-1/3}$

Rollers: $\delta_r = \frac{0.0006}{\cos \beta} l_a^{-0.8} Q^{0.9}$

Where:

δ_r = Radial displacement

δ_a = Axial displacement

F_r = Radial load

F_a = Axial load

D_w = Element diameter

l_a = Roller lengths

i = Element row number

Q = Maximal load applied on elements

The deformation for ball bearings is expressed by:

$$\delta_r = \left[10^{-4} \frac{0.002}{(\cos \beta)^{2/3}} \left(\frac{5}{10} \right)^{2/3} \right] F_r^{2/3} d_b^{-1/3} (i \cdot n)^{-2/3} \quad (29)$$

2.2 The Kramer formula

Kramer’s [9] work resulted in ball bearings stiffness k_r :

$$k_r = \frac{nF}{x_r} \tag{30}$$

Where n and x_r are given as follows:

Bearings	n	x_r
Balls	$3/2$	$1.2 \times 10^{-7} \times d^{1/3} \times Z^{2/3} \times F^{2/3}$
Rollers	$1/0.9$	$1.11 \times 10^{-9} \times l^{0.8} \times Z^{0.9} \times F^{0.9}$

Where:

- x_r = Displacement
- d = Ball diameter
- l = Roller length
- F = Load

3. Finite element analysis

Two different conditions were considered for analysis in ANSYS. Axial and radial stiffness are both analyzed. Spindle ball bearing 7014 was used as a model (fig. 7). On the basis that all the balls are distributed evenly at the circumferential direction, when the bearing is under axial displacement or force, this load will be the same to all the segments of the bearing. This presumption is called the symmetric condition. Hence one part of the whole bearing can be used to do the simulation. The result from the part model will hence be sufficient to evaluate the result.

For the case of radial load, one should consider the load distribution for the loaded balls. In other word all balls are not loaded and the loaded balls are not equally loaded (as depicted in fig. 3). This loading for the case of a radial load of 40 kN and resulting contact stress between balls and races are presented in figure 6.

A part of a ball bearing including half of a ball

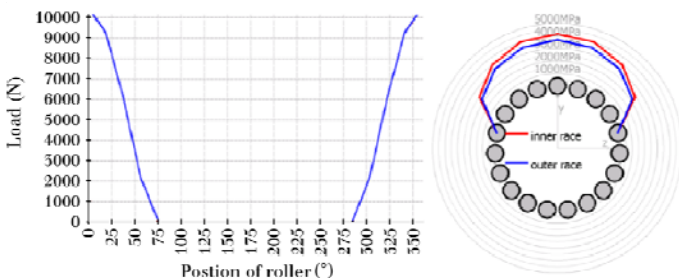


Figure 6. Loading distribution on balls of spindle ball bearing 7014 and resulting contact stress distribution

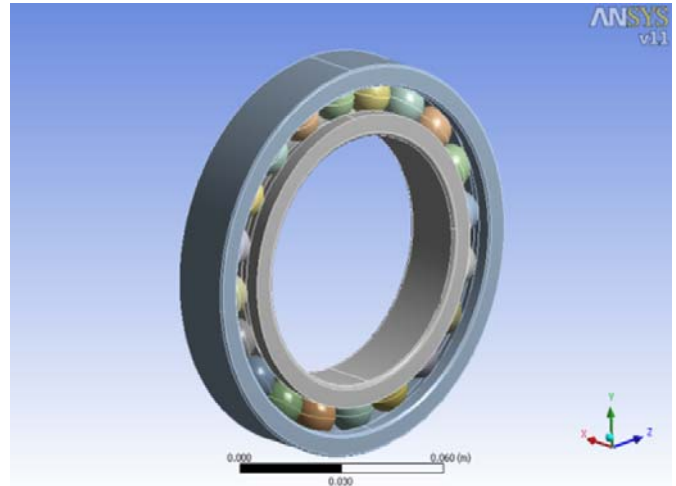


Figure 7. Spindle ball bearing 7014 in ANSYS workbench

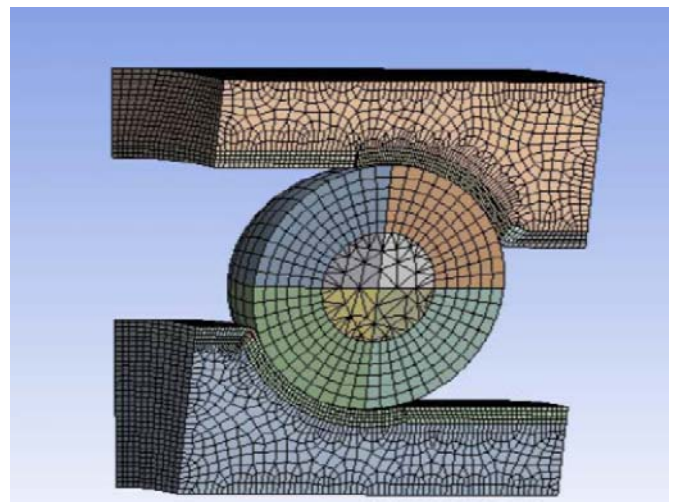


Figure 8. A simplified model of ball bearing in ANSYS

along with a slice of outer and inner ring is considered for the analysis. To do the simulation with the part model of bearing, flexible-flexible model has to be used for the rings and ball. The model is shown in figure 8. All the results of analysis were be evaluated and compared as reaction force vs. displacement of ball.

For the inner and outer ring and the outer part of the ball, SOLID 186 element as used. For the center of the ball SOLID187 was used. For the contact element, CONTA174, 3-D 8-Node Surface-Surface and for the target element, Targe170, 3-D 8-Node surface-surface were used. The materials for the inner, outer ring and balls are linear isotropic structure steel. Young’s modulus is 200 GPa and Poisson’s ratio is 0.3.

Axial loading of angular contact ball bearing causes contact between balls and races and in radial loading only some of balls are in contact with races

(fig. 6). Contact analysis in ball bearings is highly nonlinear because of geometrical nonlinearity, material nonlinearity due to stress-strain relations and status change of structural contact. Frictional contact between the ball and the raceway were chosen to do the analysis in ANSYS in order to make the solution converge better. The friction coefficient used was $\mu=0.05$.

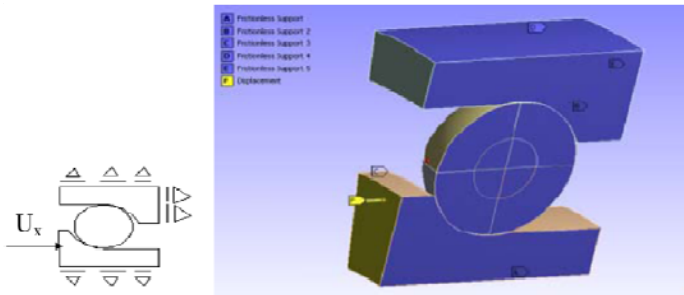


Figure 9. Boundary condition in case of axial load application in ball bearing

3.1 Boundary condition

The structure will respond differently for different boundary conditions. The boundary condition for the case of axial load analysis is depicted in figure 9. The frictionless support depicted in in figure 9 means the body can only move parallel to surface. The linear displacement of 0.1 mm in X direction (axial) and Y direction is applied onto the inner ring.

When the solution is done, it is possible to check all the parameters such as reaction force, strains and stresses, contact pressure, contact status, etc. An example of the reaction force-displacement plot of this model is depicted in figure 10.

3.2 Factors influencing the reaction force

It is of great import to consider which factors will influence the reaction force relation to displacement in order to ascertain which parameters most affect the final results of the proposed modeling. Physical parameters include the geometry, friction coefficient and the boundary conditions.

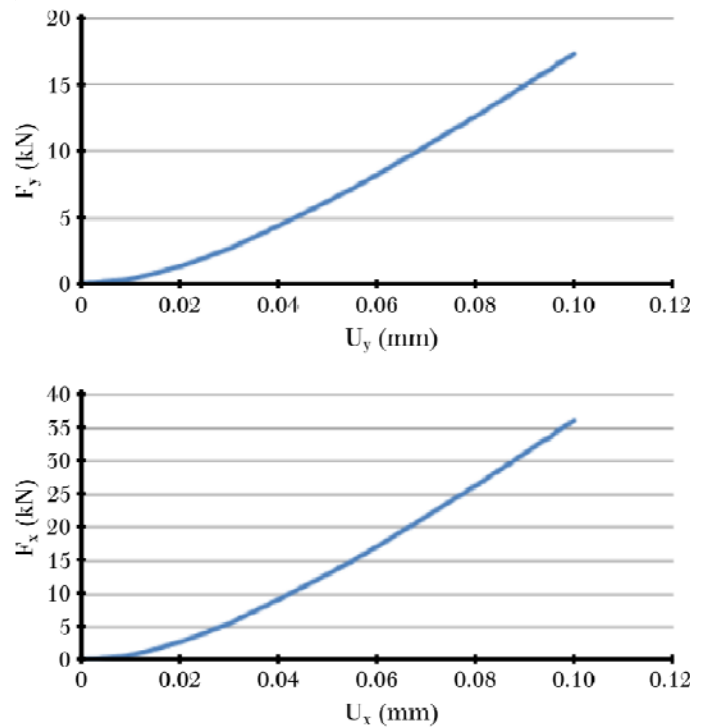


Figure 10. Reaction forces in the X and Y directions from an ANSYS simulation

Finite element analysis parameters are mesh density and penetration. These relations will be analyzed in the next steps.

The pictures shown in figure 11 are different meshes of angular contact ball bearing model. Mesh a exhibits us one coarse mesh that the mesh of races are generated automatically. mesh_b is fine but not reasonable because the elements are distorted.

Mesh_c seems to be reasonable. Further refinement of mesh_c is done in order to generate much finer mesh_d and mesh_e. The reaction force in the y direction for all the meshes are shown in figure 12.

As shown in figures 12 and 13, there exists larger difference in reaction force percent between coarse and fine mesh in the beginning region, up to

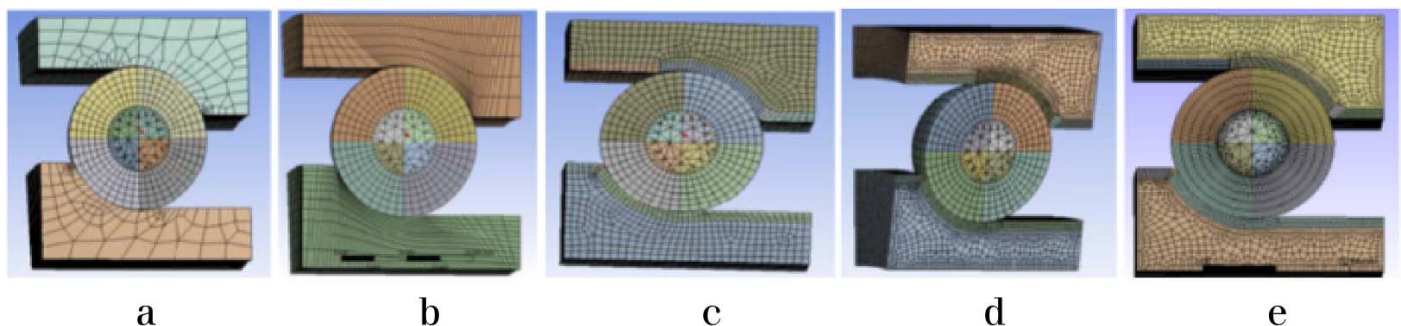


Figure 11. Models with different mesh densities

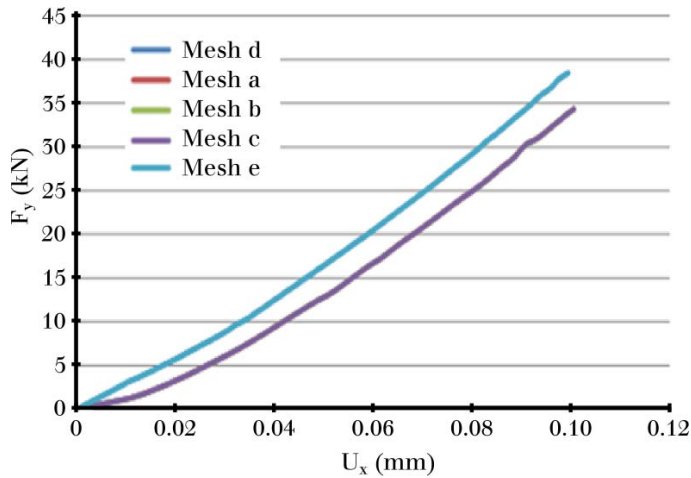


Figure 12. Reaction force comparison for different mesh densities

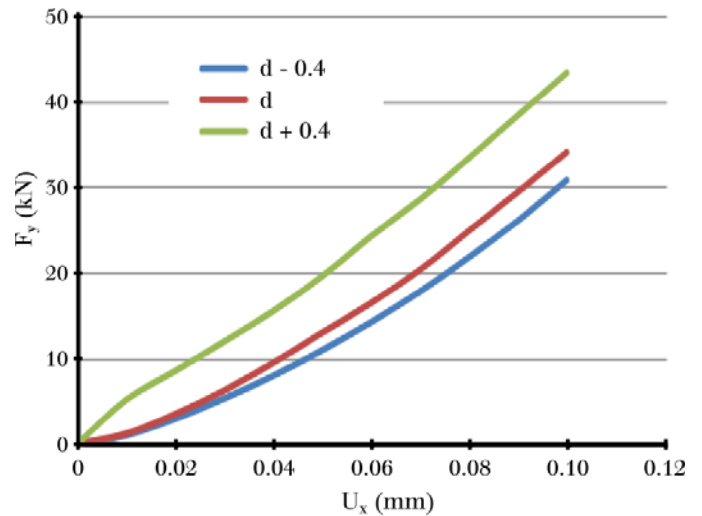


Figure 15. The effect of ball diameter on reaction force

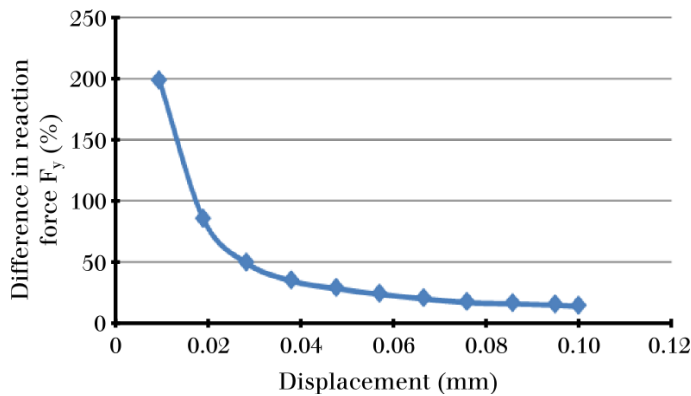


Figure 15. Difference reaction force in the Y direction for mesh_a and mesh_e

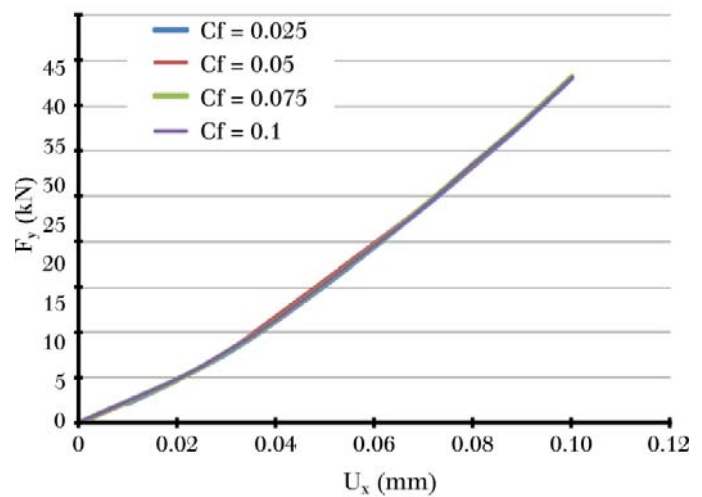


Figure 16. The effect of friction force on reaction force

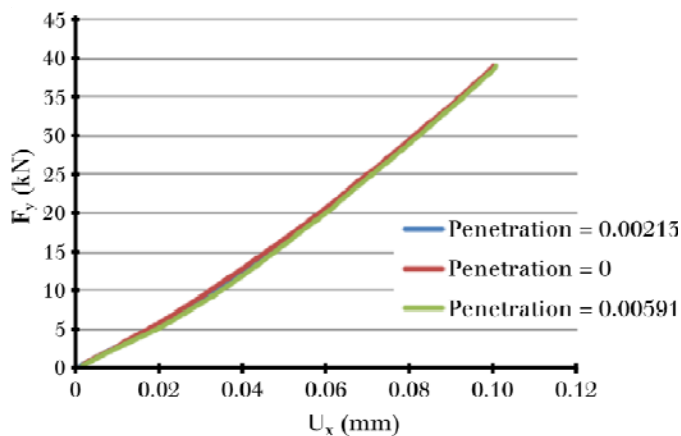


Figure 14. Penetration vs. reaction force

0.04 mm. In this region, contact stiffness has the most profound effect on the whole system stiffness. Afterwards, we find that the contact and the contact stiffness have no effect on the structural stiffness anymore, as the percent difference graph is flattened.

Penetration and Reaction Force

When the penalty based contact algorithms such as Pure Penalty and Augmented Lagrange are used to solve the contact problem penetration is a key parameter to evaluate the results of simulation in contact analysis. The ideal amount for contact penetration is zero. However, when the numerical approximation is used the penetration will be produced that should be minimized. Figure 14 plots the relation between the reaction force and different amount of maximum penetration. One can see that the penetration scarcely affects the reaction force.

Physical factors influencing the reaction force

Diameter of the balls and the curvature of the raceways of inner and outer ring, the friction coefficient and boundary condition are the physical parameters affecting the analysis results.

In the first case, the diameter of the ball is increased by 0.4 mm and in the second, the

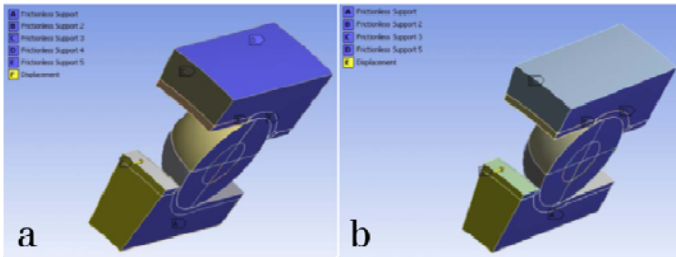


Figure 17. Different boundary conditions for outer ring. a) The outer ring is totally fixed. b) The outer ring can move in the Y direction

diameter is decreased by 0.4 mm. From figure 15 it is obvious that the diameter of the ball influences the reaction force dramatically. It is essential to make the FE model as accurate as possible: An increase of the ball diameter by 3.1% leads to the increase of reaction force by 29%. A decrease of ball's diameter by 3.1% results in the decrease of reaction force by 12.3%. Effect of friction force on the results of analysis is illustrated in figure 16.

Boundary Conditions and Reaction Force

Two cases are considered for boundary condition's effect on analysis results. The condition of the outer ring being totally fixed (fig. 17a), and the condition where the outer ring can move in the Y direction (fig. 17b).

Before doing the simulation, we sought to gauge the behavior of the structure first and then simulate it. When the result is available, it is possible to compare the simulation results (fig. 18) with the real or experimental results and find the problem. The results of two assumed boundary condition will be compared with the experimental results later to see which boundary condition is the most realistic one.

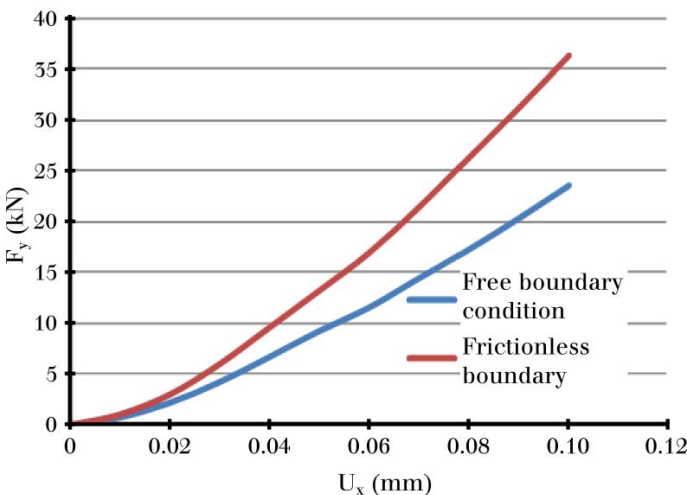


Figure 18. Boundary condition and reaction force

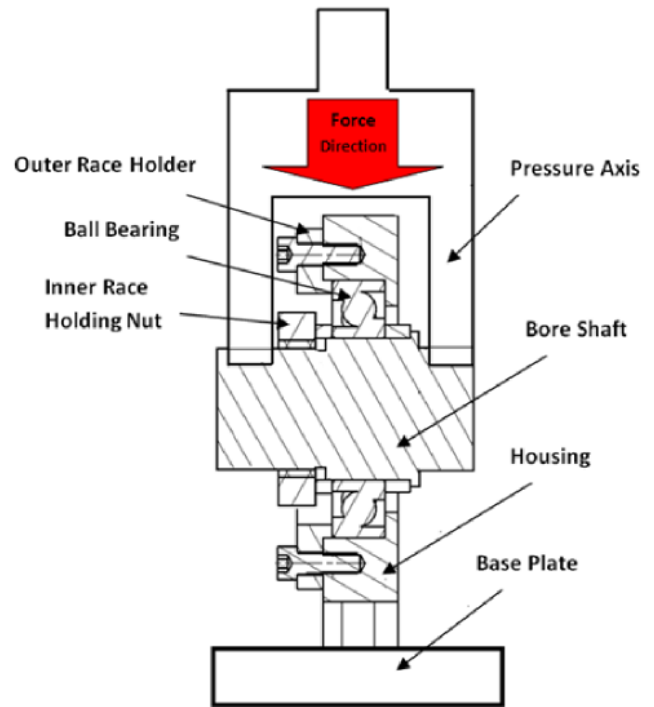


Figure 19. Testing setup: Fixture, pressure axis and ball bearing

4. Experimental validation of the model

A universal testing machine of (GOTECH) was used for tests on spindle ball bearing type SKF 7014 with 20 balls. This device is a general purpose tensile testing machine with capability of applying 100 kN on samples with a computer controlled servo system. The load was applied to the sample between stationary and moving jaws with computer-controlled speed.

Sample fixture

The structure was composed of pressure axis on the outer diameter of the bearing, and a steel rigid shaft to fit in the bore of the bearing.

The control device

The tensile machine is controllable with computer software. The test speed was adjusted and force recorded on control desk of computer. All parameters were gathered by the data acquisition system of the testing machine.

Experimental conditions

The loading speed was kept as low as possible. As the technical data sheet of the ball bearing specifies a maximum static load of below 44 kN, loading speed was set to 0.05 mm/min., the slowest in the range of the machine.

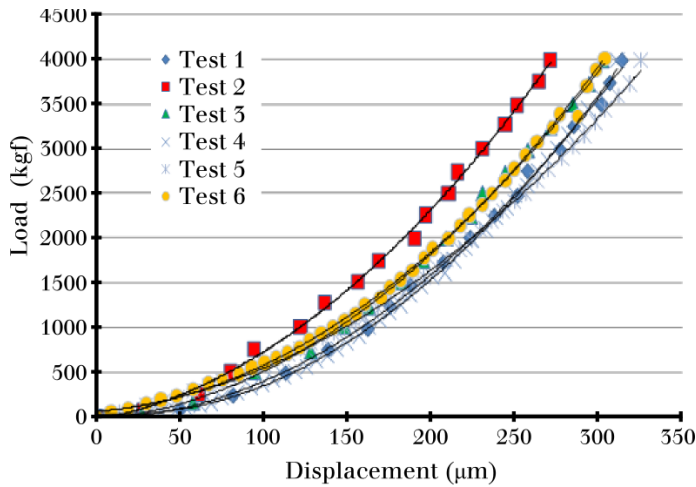


Figure 20. Test results for the loading axis crossing one ball

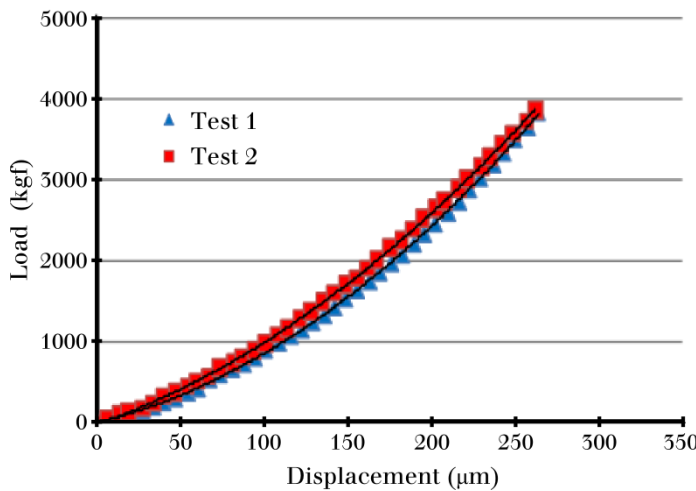


Figure 21. Test results for the loading axis crossing two balls

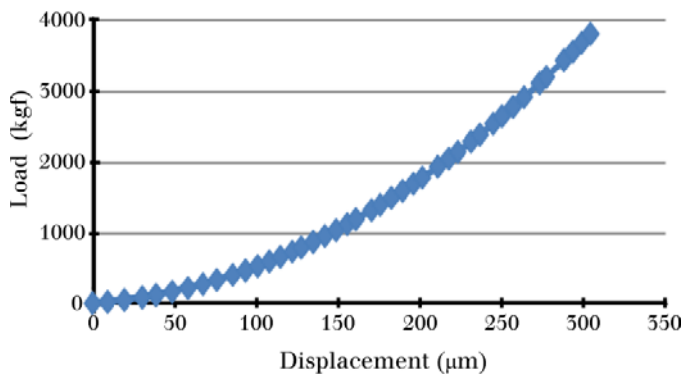


Figure 22. Average of 6 tests for the case of loading axis passing through one ball

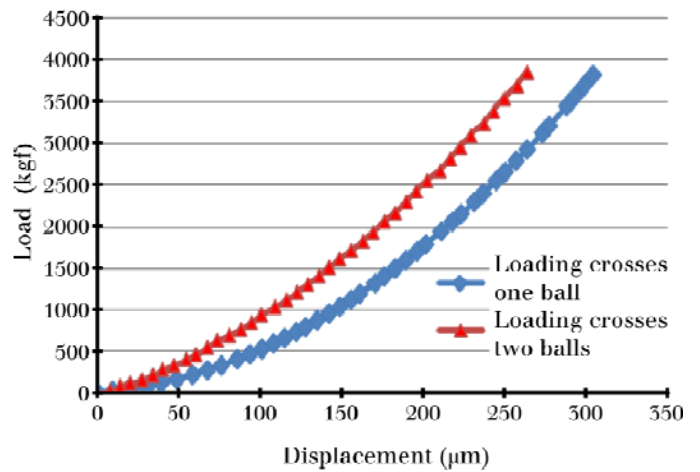


Figure 23. Comparison of test results for loading axis passes one and two balls

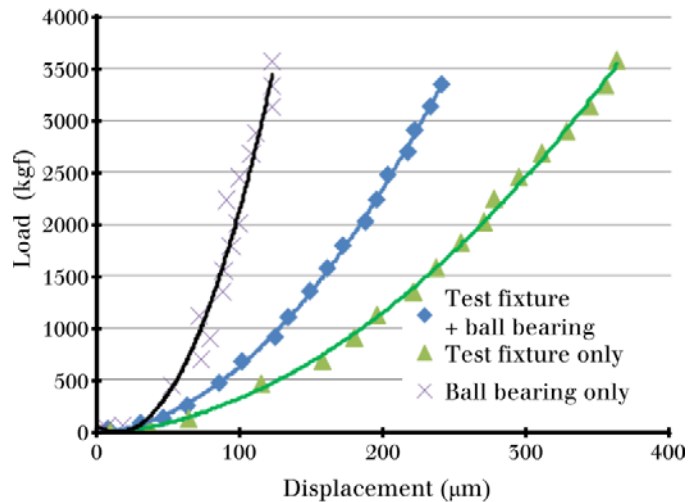


Figure 24. Ball bearing deformation deduced from tensile tests with and without the ball bearing

The ball bearing was fitted between the pressure axes and bore shaft. Tests were done in two stages. One to achieve the stiffness of the sample fixture to be subtracted from test results of (sample fixture + ball bearing). This will result in stiffness of ball bearing only.

Figure 19 shows the assembly used to measure the stiffness of ball bearing. In the first test, the loading axis passes through one ball and in the second one the loading axis crosses two balls. Six experiments (fig. 20) for the first case (the average graph is depicted in figure 22) and two experiments (fig. 21) for the later one were realized. In figure 27 a sample tensile test graph in computer is shown.

Two resulting averages for the first set of experiments are shown in figure 23. As we see the resulted stiffness of the ball bearing is a function of balls positioning. This is obvious as shown in above

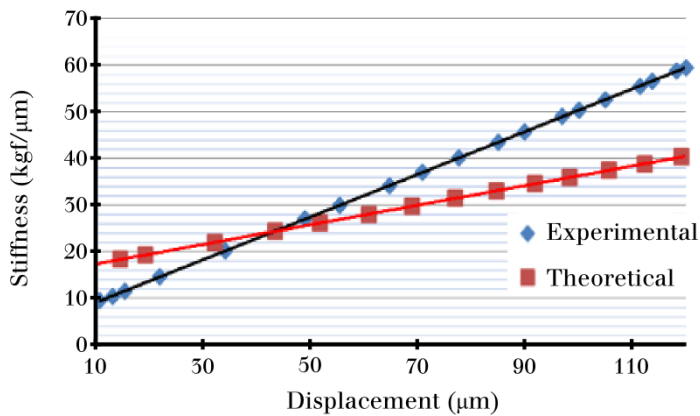
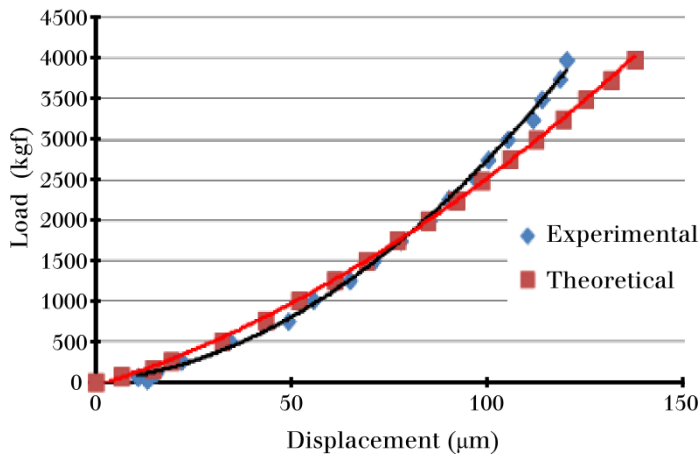


Figure 25. Comparison of theoretical and experimental curves: Load-displacement (top) and stiffness-displacement (bottom) curves

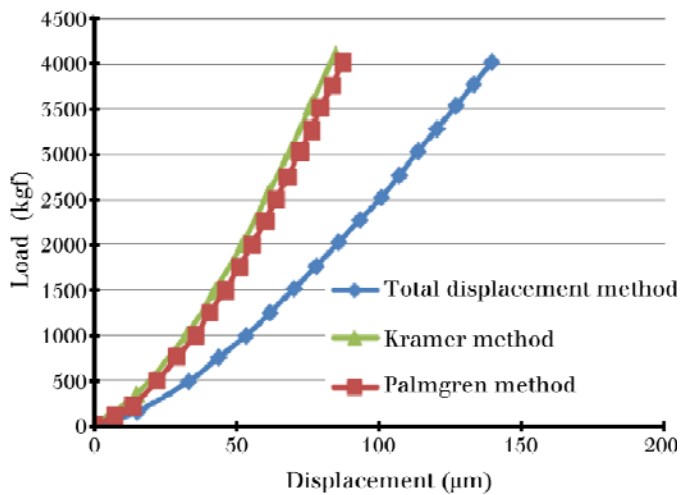


Figure 26. Theoretical method (total displacement method) comparison to Palmgren and Kramer methods

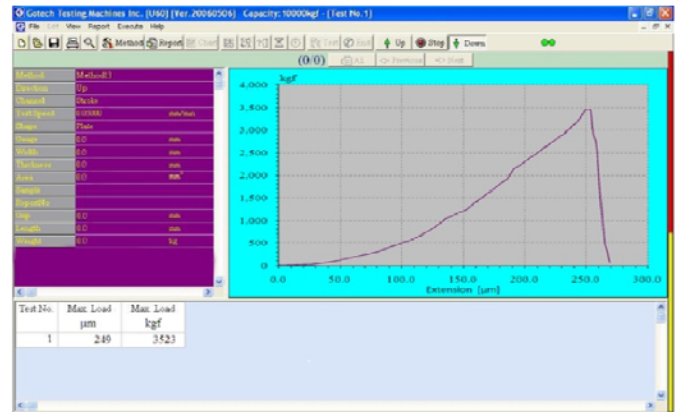


Figure 27. Sample tensile test graph obtained in GOTECH tensile testing machine

sections in theoretical formulations. As we know the resulting graphs for displacement as a function of loading for different test samples is not the actual function for the ball bearing only. The resulting displacement function includes both the displacement part of test fixtures along with the part for ball bearing. To achieve accurate results, we deduced the ball bearing displacement function from the total displacement function as follows:

We first ran a tensile test without the ball bearing in the fixture, and subsequently with ball bearing mounted in the fixture. In doing so the flexibility of the test fixture was measured and we were able to deduce the displacement function for ball bearing only. The springs (fixture and ball bearing) are considered to be in series, and the function for ball bearing deduced [25]. The resulting graphs for tensile test of (fixture only) and (fixture + ball bearing) and deduced graph for the ball bearing itself are shown in **figure 24**.

Results and discussion

The theoretical results are shown in **figure 26**. We see that by adding another displacement term to the literature formula (*i.e.* Palmgren and Kramer), the displacement value for our theoretical method based on total deformation is higher than Kramer and Palmgren for specific loading level. Six tests for the situation of loading axis passing through one ball (**fig. 20**) and two tests in the case of loading axis passing between two balls were done (**fig. 21**). We clarify the position change effect of balls on stiffness behavior of the ball bearing in **figure 23**.

Comparison between the experimental results and those drawn from the theoretical model (based on the total displacement method) is done in **figure 25**

Globally, the result from the total displacement theory reflects the experimental results relatively.

- A similarity between experimental and theoretical curves in the ball bearing working range was attained.
- At higher load values we see considerable difference in stiffness values. This may be cause of thermal heat treatment of balls and races that is not considered in theoretical models. Material nonlinearity is not considered in the model and warrants future study
- Based on good conformity between experiment and total displacement theory, FEM results can be updated for unknown parameters, for example boundary conditions, to have reliable FEM approach for stiffness analysis of ball bearings. This will omit time consuming experimental study for different types of ball bearings.
- The nonlinearity of the force-displacement curve is similar to the results of other studies [2], [9], [15] and [18].
- A difference exists for response in different cases of ball positioning. We can therefore conclude that the ball bearing stiffness changes according to the balls positioning.

Nonlinearities in the force-displacement curves are similar to the results of Flygt [12] and Kraus [15]. Results to those of Palmgren and Kramer are proximate while the total deformation curve, when we have added elastic deformation of ball to compute total deformations, is perceptibly different. Our model for nonlinear stiffness computation of a ball bearing showed good agreement with experimental values and is therefore acceptable in the range of allowable force for a ball bearing.

Works Cited

1. Shigley, J. E. and Mitchel L. D. (1985) Mechanical engineering design. 4th ed. McGraw-Hill, 85-88.
2. Palmgren, A. (1959) Ball and roller bearing engineering. 3rd ed. S. Burbank and co., Philadelphia.
3. Harris, T. A. (1991) Rolling bearing analysis. 3rd ed. Lavoisier.
4. Eschmann, P., Hasbargen, L. and Weigand, K. (1985) Ball and roller bearings theory, design and application. R, Oldenburg Verlag, John Wiley and Sons.
5. Lim, T. C. (1989) Vibration transmission through rolling element bearings in geared rotor systems. Ph.D. Thesis, Ohio State University, pp.12-60.
6. De Mul, J.M., Vree and Maas, D.A. (1989) Equilibrium and associated load distribution in ball and roller bearings loaded in 5 degrees of freedom while neglecting friction. Part I: General theory and application to ball bearings. Trans. A.S.M.E. J. Tribol., 111:149-155.

7. Fukata, S.E.H., Kondou, T., Ayabe, T., and Tamura, H. (1985) On the radial vibration of ball bearings. Bull. JSME, vol.28, 259:899-904.
8. Hentati, T. and Col, A. (2005) Finite element development for ball bearing nonlinear stiffness modelization. International Journal of Simulation Modeling, vol.4, 3:118-128.
9. Kramer, E. (1993) Dynamics of rotors and foundations. Berlin, Springer-Verlag.
10. Beatty, R.F., Rowan, B.F. (1982) Determination of ball bearing dynamic stiffness. Proceedings of a workshop on Rotordynamic Instability Problems in High Performance Turbomachinery, NASA Conference Publication 2250, 98-104.
11. Bogard, F., Debray, K., and Guo, Y.Q. (2002) Determination of sensor positions for predictive maintenance of revolving machines. International Journal of Solids and Structures, 39(12), 3159-3175.
12. Flygt / ITT Industries (2004) ITT Industries engineering for life, shaft and bearing calculations, No.02.03. Eng. 0,5 M. 04.04 892932,7-14.
13. Kraus J., Blech, J.J. and Braun, S.G. (1987) In situ determination of roller bearing stiffness and damping by modal analysis. Trans. A.S.M.E. J. Vibrat. Acoustics Stress and Reliab. Design, 109, pp.235-240.
14. Marsh, E. R., Yantek, D.S. (1997) Experimental measurement of precision bearing dynamic stiffness. Journal of Sound and Vibration , vol. 202 (1), pp. 55-66.
15. Rajab, M. D. (1982) Modeling of the transmissibility through rolling-element bearing under radial and moment loads, Ph.D. Thesis, Ohio state university, Columbus, Ohio.
16. Young, W.B.(1998) Dynamic modeling and experimental measurements of a gear shaft and housing system, M.S. Thesis, Ohio State University, Columbus, Ohio.
17. Yuzhong C. (2006) Modeling of High-speed Machine-tool Spindle Systems. Ph.D thesis, University of British Columbia, pp.20-82.
18. Yuan K., Chih-Ching H., Chorng-Shyan L., Ping-Chen S., Yeon-Pun C. (2006) Stiffness determination of angular-contact ball bearings by using neural network. Tribology International, vol 39(6), pp. 461-469.
19. El-Sayed, H.R.(1980) Stiffness of deep-groove ball bearings. Wear, Volume 65(1), pp. 89-94.
20. Guo, Y. and Parker, R.G. (2012) Stiffness matrix calculation of rolling element bearings using a finite element/contact mechanics model. Mechanism and Machine Theory, vol. 51, pp. 32-45.
21. Aydin, G., Dreyer, J.T. and Rajendra S. (2012) Effect of bearing preloads on the modal characteristics of a shaft-bearing assembly: Experiments on double row angular contact ball bearings. Mechanical Systems and Signal Processing, vol. 31, pp. 176-195.
22. Chen, Y.S., Chiu, C.C. and Cheng, Y.D. (2010) Influences of operational conditions and geometric parameters on the stiffness of aerostatic journal bearings, Precision Engineering, vol. 34(4), pp. 722-734.
23. Stone, B.J. (1982) The state of the art in the measurement of the stiffness and damping of rolling element bearings. (1982) CIRP Annals - Manufacturing Technology, vol. 31(2), pp. 529-538.
24. Harsha, S.P. (2006) Nonlinear dynamic analysis of rolling element bearings due to cage run-out and number of balls. Journal of Sound and Vibration, vol. 289(1-2), pp. 360-381.
25. Jutte, C.V. (2008) Generalized synthesis methodology of nonlinear springs for prescribed load-displacement functions. Ph.D. thesis, University of Michigan.

26. Reusner, H. (1977). *Druckflächenbelastung und oberflächenverschiebung in waltzkontakt von rotationskörpern.* SKF Kugellagerfabriken GmbH, Schweinfurt.